

Optical modeling and polarization calibration for CMB measurements with ACTPol and Advanced ACTPol

Brian Koopman^a, Jason Austermann^b, Hsiao-Mei Cho^j, Kevin P. Coughlin^g, Shannon M. Duff^b, Patricio A. Gallardo^a, Matthew Hasselfield^{c,d}, Shawn W. Henderson^a, Shuay-Pwu Patty Ho^f, Johannes Hubmayr^b, Kent D. Irwin^{j,k}, Dale Li^j, Jeff McMahon^g, Federico Nati^e, Michael D. Niemack^a, Laura Newburgh^l, Lyman A. Page^f, Maria Salatino^f, Alessandro Schillaciⁱ, Benjamin L. Schmitt^e, Sara M. Simon^f, Eve M. Vavagiakis^a, Jonathan T. Ward^e, and Edward J. Wollack^h

^aDepartment of Physics, Cornell University, Ithaca, NY 14853, USA

^bQuantum Devices Group, National Institute of Standards and Technology, 325 Broadway M.S. 817.03, Boulder, CO 80305, USA

^cDepartment of Astronomy and Astrophysics, The Pennsylvania State University, University Park, PA 16802, USA

^dInstitute for Gravitation and the Cosmos, The Pennsylvania State University, University Park, PA 16802, USA

^eDepartment of Physics and Astronomy, University of Pennsylvania, 209 South 33rd Street, Philadelphia, PA 19104, USA

^fDepartment of Astrophysical Sciences, Princeton University, Princeton, NJ 08544, USA

^gDepartment of Physics, University of Michigan, Ann Arbor, MI 48109, USA

^hNASA Goddard Space Flight Center, Greenbelt, MD 20771, USA

ⁱInstituto de Astrofísica and Centro de Astro-Ingeniería, Facultad de Física, Pontificia Universidad Católica de Chile, Santiago, Chile

^jSLAC National Accelerator Laboratory, 2575 Sandy Hill Road, Menlo Park, CA 94025, USA

^kDepartment of Physics, Stanford University, Stanford, CA 94305-4085, USA

^lDunlap Institute, University of Toronto, Toronto, Ontario M5S 3H4, Canada

ABSTRACT

The Atacama Cosmology Telescope Polarimeter (ACTPol) is a polarization sensitive upgrade to the Atacama Cosmology Telescope, located at an elevation of 5190 m on Cerro Toco in Chile. ACTPol uses transition edge sensor bolometers coupled to orthomode transducers to measure both the temperature and polarization of the Cosmic Microwave Background (CMB). Calibration of the detector angles is a critical step in producing polarization maps of the CMB. Polarization angle offsets in the detector calibration can cause leakage in polarization from E to B modes and induce a spurious signal in the EB and TB cross correlations, which eliminates our ability to measure potential cosmological sources of EB and TB signals, such as cosmic birefringence.

We calibrate the ACTPol detector angles by ray tracing the designed detector angle through the entire optical chain to determine the projection of each detector angle on the sky. The distribution of calibrated detector polarization angles are consistent with a global offset angle from zero when compared to the EB-nulling offset angle, the angle required to null the EB cross-correlation power spectrum. We present the optical modeling process.

The detector angles can be cross checked through observations of known polarized sources, whether this be a galactic source or a laboratory reference standard. To cross check the ACTPol detector angles, we use a thin film

Further author information: (Send correspondence to B.K.)

B.K.: E-mail: bjk98@cornell.edu, Telephone: 1 607 255 0833

polarization grid placed in front of the receiver of the telescope, between the receiver and the secondary reflector. Making use of a rapidly rotating half-wave plate (HWP) mount we spin the polarizing grid at a constant speed, polarizing and rotating the incoming atmospheric signal. The resulting sinusoidal signal is used to determine the detector angles.

The optical modeling calibration was shown to be consistent with a global offset angle of zero when compared to EB nulling in the first ACTPol results and will continue to be a part of our calibration implementation. The first array of detectors for Advanced ACTPol, the next generation upgrade to ACTPol, will be deployed in 2016. We plan to continue using both techniques and compare them to astrophysical source measurements for the Advanced ACTPol polarization calibration.

Keywords: Cosmic Microwave Background, polarization, ACTPol, detector angle

1. INTRODUCTION

The Atacama Cosmology Telescope (ACT) is an off-axis Gregorian telescope constructed in 2007.¹ The Atacama Cosmology Telescope Polarimeter (ACTPol) is a polarization sensitive receiver upgrade to ACT. Starting in 2013, in a staged deployment, ACTPol began observing the Cosmic Microwave Background (CMB). In the most recent observation season ACTPol used $\sim 3,000$ transition edge sensor bolometers, in two frequency bands across three arrays.²

The primary elements of the ACTPol optical chain are a 6 m primary mirror, a 2 m secondary mirror and three optics tubes, each of which contains a set of three silicon reimaging lenses. Other elements include the receiver window, several band defining filters and a set of corrugated feedhorns per array. Figure 1 shows the optical chain with a simple ray trace for one optics tube.

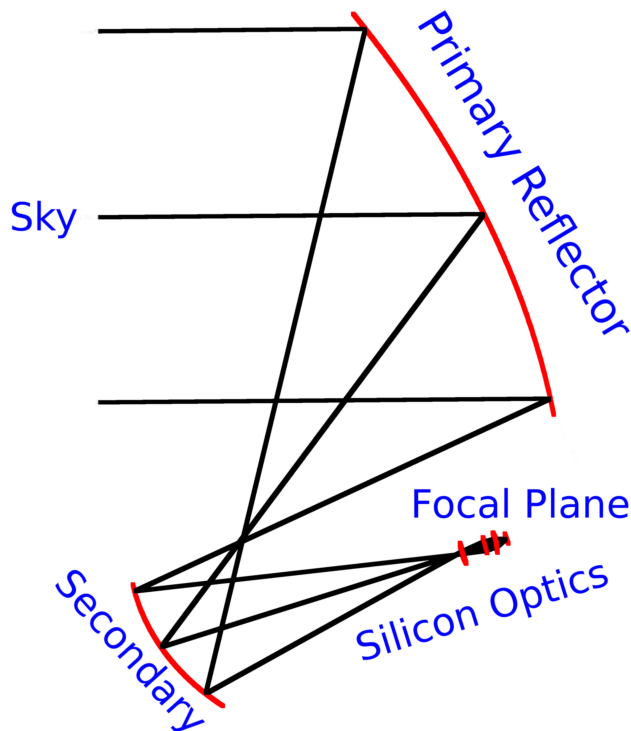


Figure 1. Single field ray trace of the ACTPol optics. Shown here is a simple ray trace from CODE V, with a single field point on the sky propagated to the primary mirror, secondary mirror, and through the refractive silicon optics in the ACTPol receiver for a single optics tube. The focal plane for one array is the final element, where the ACTPol detectors lie.

The corrugated feedhorns each couple to an orthomode transducer (OMT) which separates incoming light into orthogonal polarizations. The angle of the two OMT fins are defined by lithography in fabrication. The ACTPol detectors are fabricated on 3-inch wafers which were etched into hexagonal and partial hexagonal shapes (referred to as “hexes” and “semi-hexes”) and tiled in an array of three hexes and three semi-hexes each. The orthogonal antenna probes on each wafer are oriented at 0/90 degrees and 45/135 degrees, such that the full array of six wafers has sets of detectors ranging from 0 to 180 degrees at 15 degree intervals.

The initial set of calibration angles are determined by the photolithography of the detector wafers and their placement into the array. We then add an array-specific angle when the array is installed into the receiver cryostat. This angle is constrained mechanically, hereafter referred to as the “installation angle.” Finally, the optics chain itself (the reflectors and lenses) causes a position dependent polarization rotation, which we solve for using the optical design software CODE V*. All three of these angles are combined to produce the final polarization angle calibration for ACTPol.

2. POLARIZATION CALIBRATION AND COSMIC POLARIZATION ROTATION

Cosmic polarization rotation (CPR), also referred to as “cosmological birefringence,” is the rotation of linearly polarized light as it traverses empty space at cosmological scales.^{3,4} The search for a non-zero CPR is a test for CPT-violating physics and has been probed across the electromagnetic spectrum with observations of polarized radio and UV emission from galaxies, polarized gamma ray bursts and the CMB polarization signal.^{4–8}

The best constraints on CPR today come from observations of the polarization of the cosmic microwave background (CMB).⁹ The CMB can be used to put constraints on CPR through the cross-correlation power spectra. CMB temperature and polarization maps can be expanded in the spherical harmonics $Y_{\ell m}^X$. The covariances of the corresponding expansion coefficients $a_{\ell m}^X$ form the angular power spectra,

$$C_{\ell}^{XX} \delta_{\ell\ell'} \delta_{mm'} = \langle a_{(\ell m)}^{X*} a_{(\ell' m')}^X \rangle, \quad (1)$$

where XX can be any combination of T , E , B (e.g. TT , EE , BB , TE , TB , EB).^{10,11} The distribution of inhomogeneities in the CMB are required to be invariant under parity and since $Y_{\ell m}^T$ and $Y_{\ell m}^E$ have parity $(-1)^\ell$ and $Y_{\ell m}^B$ has parity $(-1)^{\ell+1}$ we expect $C_{\ell}^{TB} = 0$ and $C_{\ell}^{EB} = 0$.¹⁰ A non-zero CPR angle would cause a mixing of E-modes into B-modes, resulting in non-zero EB and TB cross-correlation power spectra ($C_{\ell}^{'TB}$, $C_{\ell}^{'EB} \neq 0$).³ The amount of mixing caused by a CPR rotation, α , is given as,^{3,12,13}

$$C_{\ell}^{'TE} = \cos(2\alpha) C_{\ell}^{TE}, \quad (2)$$

$$C_{\ell}^{'EE} = \sin^2(2\alpha) C_{\ell}^{BB} + \cos^2(2\alpha) C_{\ell}^{EE}, \quad (3)$$

$$C_{\ell}^{'EB} = \frac{1}{2} \sin(4\alpha) (C_{\ell}^{BB} - C_{\ell}^{EE}), \quad (4)$$

$$C_{\ell}^{'TB} = -\sin(2\alpha) C_{\ell}^{TE}, \quad (5)$$

$$C_{\ell}^{'BB} = \cos^2(2\alpha) C_{\ell}^{BB} + \sin^2(2\alpha) C_{\ell}^{EE}. \quad (6)$$

Here the primes on the left side indicate the observed, rotated, power spectra. The non-primed terms give the original, unrotated, quantities. Looking at Equations (4) and (5), we see that a non-zero EB and TB power spectrum can result from a mixing of E into B modes.

Any miscalibration in the detector angles of an experiment is degenerate with a non-zero CPR. As a result, current constraints on α are limited by the systematic error associated with calibrating the polarization angle of the detectors. Current polarization techniques limit the angular resolution to roughly $\pm 0.5^\circ$.⁹ In addition, using the assumption that $C_{\ell}^{'TB}$ and $C_{\ell}^{'EB} = 0$ to determine the calibration angle eliminates the ability to measure a DC CPR.

*Synopsis Optical Solutions Group – <https://optics.synopsys.com/codev/>

3. OPTICAL MODELING CALIBRATION

The ACTPol telescope and receiver design was modeled with the optical design software CODE V. Using CODE V we model the ACTPol telescope, perform a ray trace to construct a function which transforms focal plane coordinates to coordinates on the sky, and finally use a polarization sensitive ray trace to calculate polarization rotations caused by the optics. Together, they provide a final polarization angle calibration for each detector on the focal plane, which forms a critical input to the map making process.

3.1 Ray Tracing

As described in Section 1, the starting point for our calibration is the lithographically defined angles for each detector. Tiled into an array these populate every 15 degrees from 0 to 180 degrees. Table 1 shows the distribution of angles for each array. The tiled detectors all lie behind a nanofabricated set of corrugated feedhorns whose positions are known precisely, which establishes a set of focal plane coordinates. These focal plane coordinates, coupled with the detector angles, form our initial parameters. All rotations are applied to these angles to produce our final angle calibration.

Table 1. Distribution of detector angles in focal plane coordinates for all three ACTPol arrays.

Angle	PA1	PA2	PA3
0°	87	80	86
15°	87	87	76
30°	80	87	86
45°	87	79	84
60°	87	87	78
75°	79	87	84
90°	87	80	86
105°	87	87	76
120°	80	87	86
135°	87	79	84
150°	87	87	78
165°	79	87	84

The first step in our calibration is to determine the installation angle, which is a global rotation of the detectors as an array is installed into the ACTPol receiver. This installation angle is different for each array and arises due to mechanical constraints within the receiver. Observations of Saturn and Uranus are fit to a 2D Gaussian per detector, which gives us pointing information for each feed and allows us to determine the installation angle. Knowing where each detector is in sky coordinates allows one to construct a scaling to take the focal plane coordinates to sky coordinates. A global rotation can then be applied to match the observed sky coordinates. This global rotation does not take into account smaller position and rotation angle distortions caused by the optical chain. We can recover these optical distortions with CODE V.

CODE V is an optical ray trace code that we use to trace the sky through the optics to the focal plane. CODE V allows a user to set up to 25 input fields at a time. The code traces each of the 25 input sky fields through the reflectors and lenses back to the feed horns. The final ray trace provides a mapping between the coordinates on the sky and position on the focal plane. The point spread function (PSF) for each field is then computed, returning the PSF centroid relative to the chief ray coordinates returned by the real ray trace. The locations of each PSF centroid are combined with the real ray trace results to form a final focal plane coordinate per input field. The 25 fields are then fit to a 2D quadratic in x and y , shown as $f(x, y)$ in Equation (7), where x and y are in focal plane coordinates. This produces two functions to transform focal plane coordinates to sky coordinates, one for x_{sky} and one for y_{sky} .

$$f(x, y) = A + Bx + Cy + Dx^2 + Exy + Fy^2 \quad (7)$$

These fits are then used to propagate each feedhorn location to the sky. This incorporates any optical distortions on the positions caused by the ACTPol optics to 2nd order and is a clear improvement over a simple scaling. Given the focal plane coordinates for each feedhorn in an array we then propagate those coordinates to the sky and perform a least squares minimization, allowing a global translation and rotation, to match the modeled sky coordinates to those determined for each feedhorn by planet observations.

Figure 2 (left) shows a plot of the PA2 focal plane coordinates propagated to sky coordinates using the fit to the CODE V model along with the determined detector positions from planet observations. The least squares minimization has been performed and for PA2 returns a required rotation of 23.1 degrees from our initial focal plane coordinates for that array. This forms our installation rotation and is applied globally to all detector angles in the array. Figure 2 (right) shows a histogram of the differences in position per feed horn after least squares minimization for PA2 using a simple scaling versus using the CODE V model, showing we can model the position angle of each detector to better than $20''$.

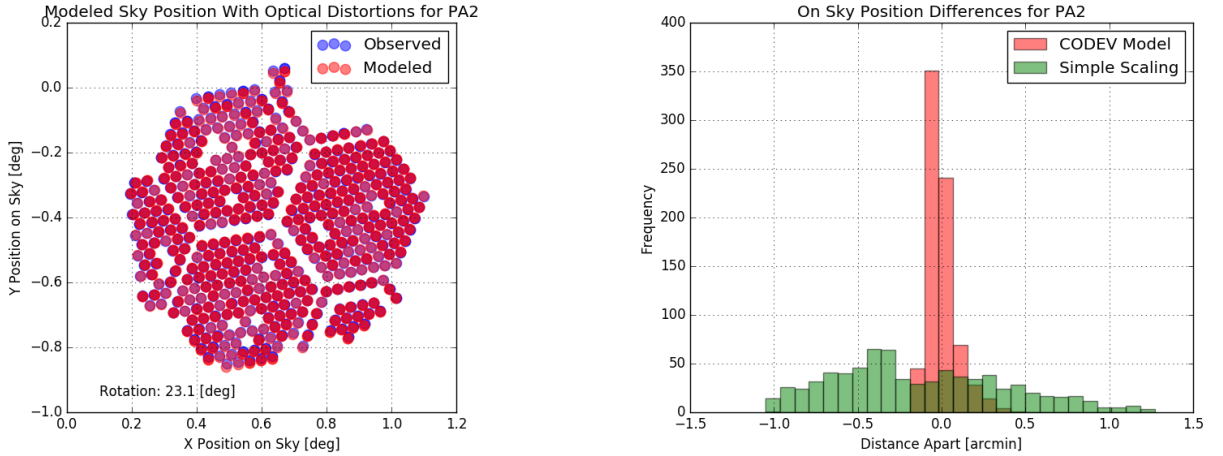


Figure 2. (Left): Feedhorn locations in sky coordinates as determined by planet observations (Observed in blue) and by ray tracing in CODE V (Modeled in red). The CODE V modeling locations are computed using the fit to the ray trace and point spread functions given by Equation (7). (Right): Histogram of differences between observed and modeled detector positions on the sky, calculated for a simple scaling to transform focal plane coordinates to sky coordinates (green) and for the CODE V modeled ray trace (red).

3.2 Polarization Rotation

The next step in the calibration is to calculate polarization rotation caused by the ACTPol optics. CODE V is capable of performing a polarization sensitive ray trace that can compute the transmittance at each surface from the Fresnel equations. We define the input polarization field to be identical for each sky trace and then use the poldsp MACRO[‡] to calculate the polarization state for nineteen rays across the entrance pupil diameter. The average polarization across the entrance pupil diameter is then computed per field.

This set of polarization rotations is used in another 2D quadratic fit using Equation (7), similar to what was done to transform the focal plane coordinates to sky coordinates. The fit results are then used to calculate the rotation associated with each feedhorn position on the focal plane. This is performed for the entire optical chain, producing the polarization rotations for each feedhorn, which are then combined with the initial angle and installation angle to produce a final calibration angle per detector. The left side of Figure 3 shows the resulting polarization rotation across the PA2 focal plane plotted in sky coordinates. To show the distribution of rotations due to just the telescope mirrors the right side of Figure 3 shows the polarization rotation at the telescope focus for PA2.

[‡]poldsp is a user supplied MACRO written by members of the Physics Department at the University of Alabama, Huntsville which supplements the polarization output from CODE V.

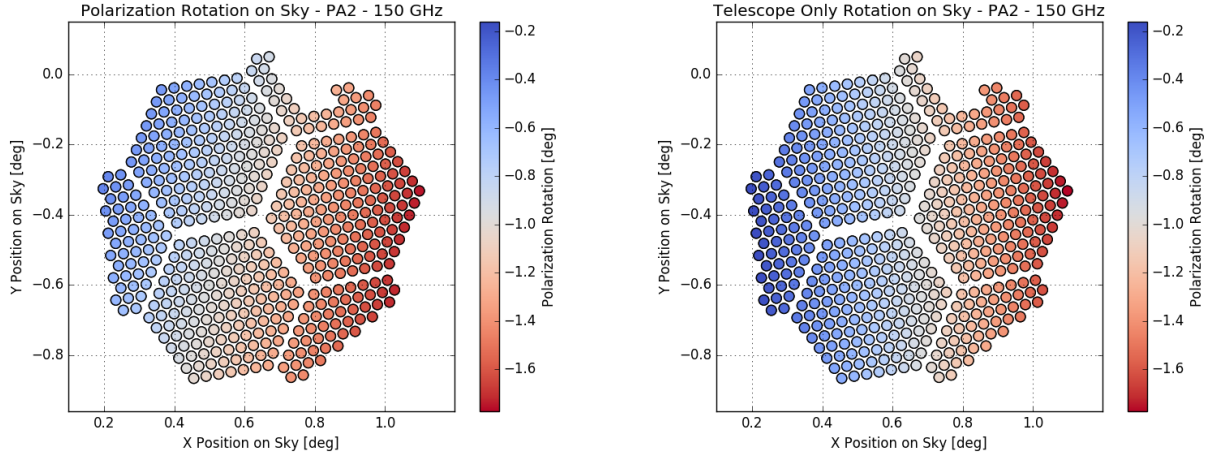


Figure 3. (Left): Polarization rotation across the PA2 focal plane for the entire optical chain at 146 GHz as determined by CODE V, plotted in sky coordinates. (Right): Polarization rotation from the ACTPol reflectors only. The final surface in this calculation is the focus. Note that the reimaging optics introduce a rotation.

Accounting for the anti-reflection coatings on the ACTPol optics is important in properly modeling the polarization rotation. The lenses are off-axis and thus influence the propagation of the polarization vectors through the camera according to their Fresnel coefficient. ACTPol uses multilayer metamaterial anti-reflection (AR) coatings on each lens in the optical chain.¹⁴ These multilayer coatings are entered in CODE V using a multilayer coating definition file (MUL), defining their thickness and index of refraction. For the ACTPol coatings, we used physically measured thicknesses and HFSS simulated effective indices for the coating parameters. These parameters are shown in Table 2.

Table 2. Coating parameters used to model the 2-layer and 3-layer anti-reflection coatings applied to the ACTPol lenses. The index of refraction for the silicon substrate is modeled to be 3.384 for all lenses.¹⁴

	Thickness [μm]	Index
2-Layer	365	1.38
	200	2.50
3-Layer	470	1.28
	315	1.95
	245	2.84

Calculating the polarization rotation for many different wavelengths across the ACTPol science band shows the wavelength dependence of the rotations caused by the optics. Figure 4 shows this for PA3, the multi-chroic array in ACTPol. The polarization rotation is uniform across frequencies within the highlighted science bands, where the AR coating parameters are tuned for maximum transmission. Figures 3 and 4 show that the refractive optics reduce the total range of polarization rotations in band across the focal plane.

3.3 Optical Modeling Results

Working from the initial, lithographically defined, detector positions and polarization angles we apply the series of calibration rotations detailed above to form a final polarization angle calibration per detector for making maps of the CMB polarization. The final ACTPol detector angle calibrations are shown in Figure 5, with colors and marker shape indicating with and without the CODE V correction for the polarization angle.

This CODE V angle, while small, has been critical in calibrating the detectors for ACTPol. Results published from the first season of ACTPol data used polarization angles derived from the prescription outlined in this

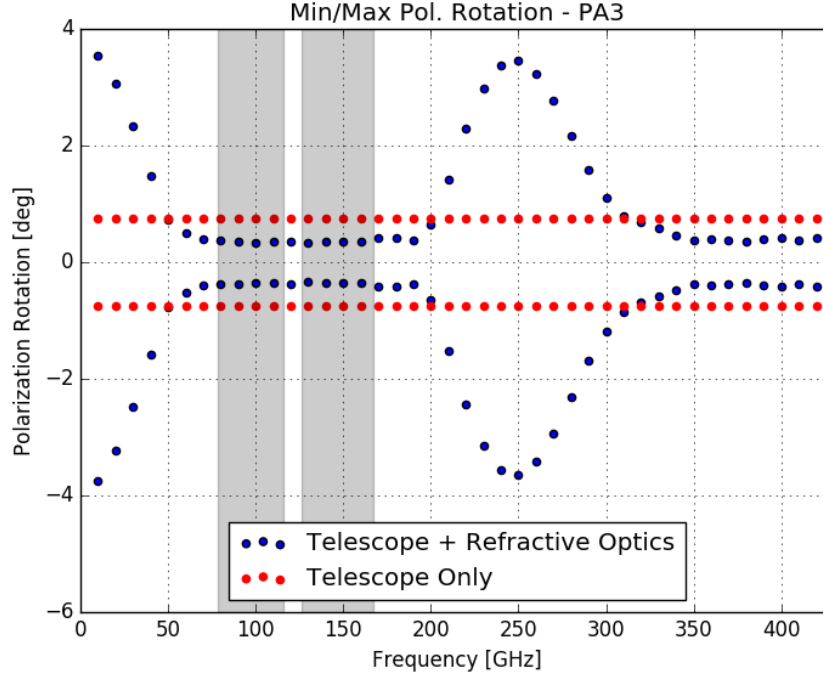


Figure 4. Plot of the minimum and maximum polarization rotations caused by the ACTPol optical chain as a function of frequency of the incoming light. Plotted in red are the minimum and maximum polarization rotation contributions from the telescope mirrors only, terminating at the receiver window. Plotted in blue are the minimum and maximum polarization rotations for the entire optical chain, including the anti-reflection coated silicon refractive optics. Highlighted in gray are the upper and lower science bands for CMB observations with PA3. Polarization rotation is similarly uniform across the science bands for PA1 and PA2.

proceedings, and checked the results by measuring the EB cross-spectrum. The EB nulling angle was found to be consistent with zero, $\delta\gamma_p = -0.2^\circ \pm 0.5^\circ$, implying that the polarization angle calibration by optical modeling works at the 0.5° level or better.¹⁵

4. POLARIZATION GRID CALIBRATION

We built a thin film polarization grid to directly measure the polarization rotation caused by the optics. The polarization grid was placed at the entrance to the receiver and used to polarize the input to the receiver. This procedure is used to extract a per detector polarization angle and is compared to the optics only polarization rotation as determined in CODE V.

4.1 Polarization Grid Design

A large, rapidly modulating, polarized signal on the detectors would drive the detectors into a nonlinear regime. With this in mind we explored different polarization grid geometries using CST Microwave Studio[§], varying the wire pitch and width for a given material thickness to produce a mostly reflective grid. This would produce a small polarized signal on the detectors so that they remain stable during measurements.

The grid is a thin metal film on a PolyEthylene Terephthalate (PET) substrate, $12\mu\text{m}$ thick (48 gauge), sourced from Dunmore Corporation[†]. The PET is fully metalized on one side with 30 nm of aluminum. The

[§]<https://www.cst.com/products/cstmws>

[†]<http://www.dunmore.com>

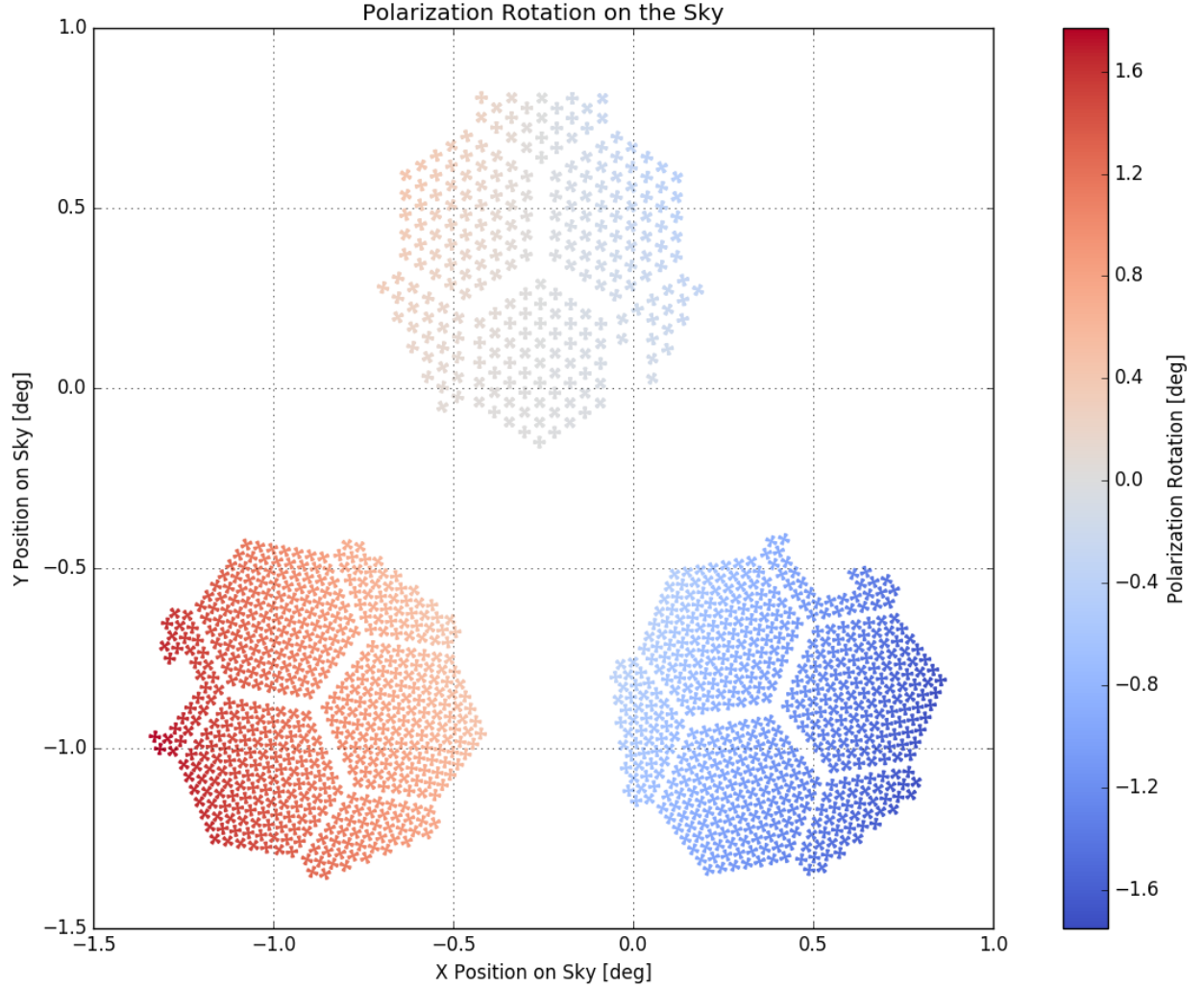


Figure 5. Plot of all three ACTPol arrays in sky coordinates. The angles of the plotted points correspond to the physical angle of the detectors in the telescope. The color scale corresponds to the additional polarization rotation caused by the ACTPol optics that is required to complete the angle calibration. This additional -1.7 to 1.7 degree rotation has been an important input to the detector angle calibration in published ACTPol results.

desired geometry is then made through laser ablation of the aluminum layer by PhotoMachining Inc.* Based on simulations in CST Microwave Studio, we chose a geometry of straight, parallel wires, $950\ \mu\text{m}$ wide, on a $1000\ \mu\text{m}$ pitch.

This produces a grid with 97% reflection in one polarization and 99.8% in the other polarization at 150 GHz, as determined by CST Microwave Studio. We measured the reflectance of the grids to be $95 \pm 5\%$ reflective in one polarization, $90 \pm 7\%$ in the other polarization at 150 GHz using a custom reflectometer setup at the University of Michigan.

*<http://photomachining.com>

4.2 Polarization Grid Assembly and On Telescope Performance

The polarization grid was attached to a simple aluminum ring, the same thickness as the planned Advanced ACTPol half-wave plates, to fit into the half-wave plate mounting hardware. We built a simple mounting stand to attach the grid to the aluminum ring. Figure 6 (left) shows the polarization grid stand; the grid was securely attached to an aluminum panel with a circular cutout. The aluminum ring was then epoxied and raised into the PET side of the polarization grid, providing tension while the epoxy set. Two polarization grids were successfully mounted using the test stand, one for each of the two 150 GHz optics tubes on ACTPol.

The polarization grids were individually installed into the Advanced ACTPol half-wave plate mounts on the front of the telescope receiver. The half-wave plate mounting hardware contains an air bearing, allowing the mounted polarization grids to spin friction free. Coupled with an external motor the polarization grids were spun at 0.5, 1 and 2 Hz during measurements. Several sets of measurements were performed at these three constant rotational rates, rotating both clockwise and counter clockwise. During measurements, the telescope remained stationary.

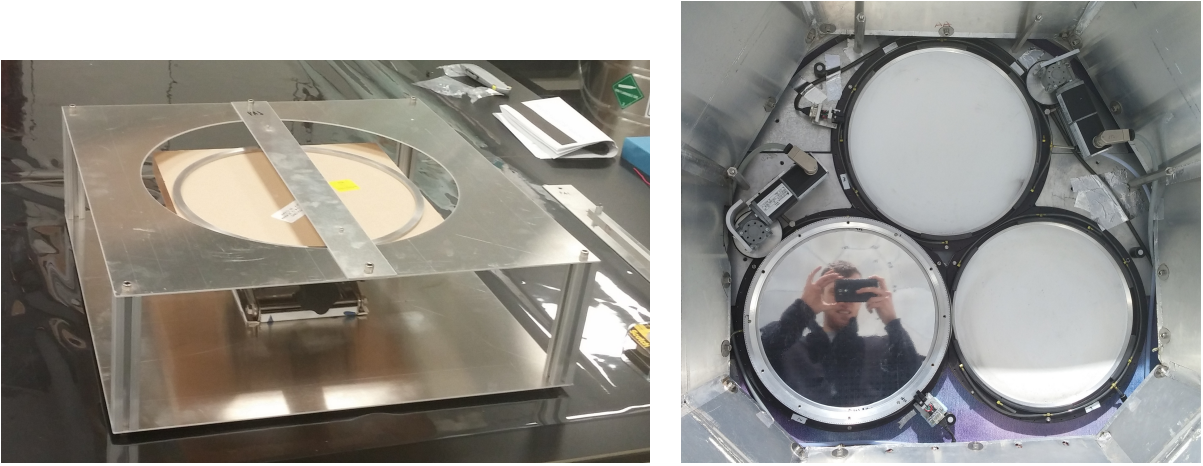


Figure 6. (Left): Polarization grid mounting and alignment stand. The polarization grid is taped taut across the round opening and aligned using the pictured cross bar using alignment marks on the grid to alignment holes on the aluminum mounting ring. The aluminum ring is epoxied and raised into the grid, making it taut and smooth. The epoxy is allowed to set and then excess material is removed. (Right): Photo of the front of the ACTPol receiver. The arrays are numbered 1-3 starting with the bottom right and moving clockwise. As pictured here PA1 and PA3 have nothing installed in front of them, PA2 has the thin film polarizing grid installed. The motor seen up and to the left of the polarization grid on PA2 rotates the grid which is floating on an air bearing. The encoder, in the bottom right, and the associated readout electronics (not pictured) record the angular position of the grid during rotation.

The right panel of Figure 6 shows one of the polarization grids installed on PA2, the second ACTPol array. With the grid rotating at a constant rate, the detectors see a sinusoidal signal. On short time scales the amplitude of the sinusoidal appears constant. Over the length of a single five minute measurement the amplitude varies with changes in the atmosphere. We only need to extract the phase from the sine wave in order to determine the polarization angles of the detectors. Before performing a fit to extract the phase we normalize and then band-pass filter the raw detector time streams with a 0.5 Hz wide Butterworth filter centered on twice the grid rotation frequency. The filtering damps low frequency atmospheric oscillations as well as high frequency harmonics.

We use the phase determined from the time stream fits to calculate the angle of each detector. Two detectors that are 180° out of phase are orthogonal so the detector angles are calculated as their phase angle divided by two. The coordinate system for the measured detector angles is set by the angular position of the polarization grid at the start of a time stream. Without knowledge of the angular position of the grid, we globally rotate the determined angles relative to a single reference detector's physical coordinate system determined by the optical modeling calibration without additional rotations due to the optics from CODE V. This zeros the measured angle for that single detector and makes all other measured angles relative to the chosen detector's local coordinate

system. Figure 7 shows the physical angles of the detectors on the sky and the measured angles from the time stream fits.

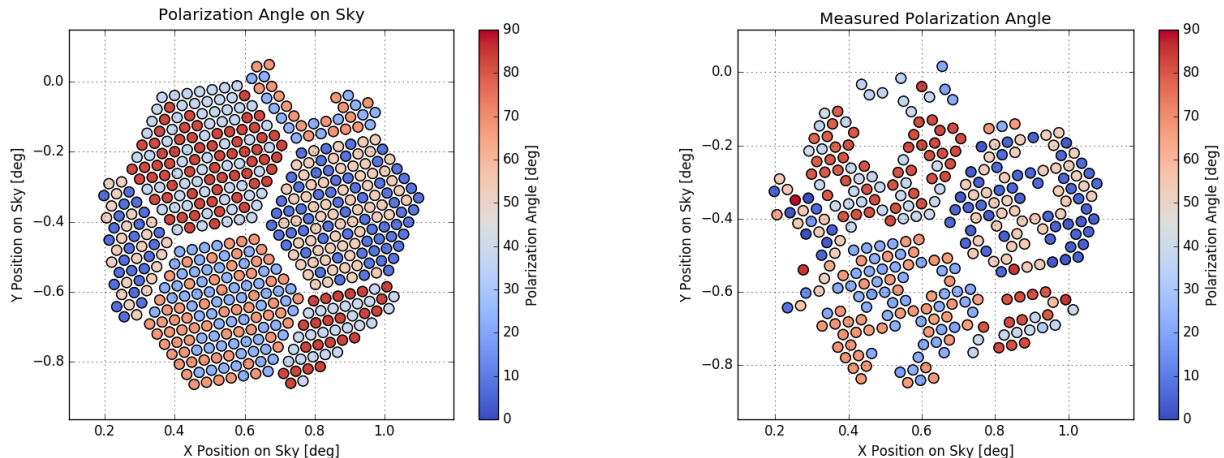


Figure 7. (Left): Physical detector angles for each detector pair projected on the sky. The color bar describes the angles of one of the detectors in each feedhorn, the other detector being orthogonal to the one plotted. (Right): Measured polarization angles from the polarization grid data sets. Like in the left panel, each circle represents a feedhorn which contains a pair of detectors orthogonal to one another. The color bar describes the angle of a single detector in the feed. Feeds are missing here, causing gaps when compared to the left panel, if they are missing a single detector in the pair due to less than 100% yield in the array.

We then subtract the measured relative angles with the physical angles of the detectors in the receiver. This produces a measurement of polarization rotation due to the optics. This can be illustrated by subtracting the two plots in Figure 7, producing a plot similar to the left plot of Figure 8. Based on modeling in CODE V the polarization rotation appears to be independent of input polarization angle, so we then average the measured polarization rotation determined for colocated detectors, which gives a measured polarization rotation per feedhorn. We again rezero by removing the averaged phase for our selected feedhorn from all feeds. The polarization angles can then be explored by selecting different zeroing detectors across the focal plane.

The results for a single chosen detector are shown in Figure 8. For the selected reference detector coordinate system the average difference from the physical angles for all the detectors across the focal plane is -0.4 ± 2 degrees. The mean is dependent on which detector we choose as a reference, while the standard deviation, reported as the error, is independent of the choice of reference.

There are still improvements to be made with the polarization grid measurements. When fabricated, the grid was ablated in small, roughly 1" by 1" square sections. While many sections are aligned, some are misaligned by as much as $\sim 25 \mu\text{m}$. This means the wires are not uniformly straight across all areas of the grid. It is evident that the uniformity of the grid greatly affects our ability to determine the detector angles. Defects in the wire alignment that are radially separated by 90° may lead to the observed differences in the measured relative angles of colocated detectors, which show minimal differences in modeling.

Defects in the grid can also arise in mounting. Imperfections in mounting manifest themselves as wrinkles across the grid. Coupled with small vibrations from the surroundings (i.e. wind, the HWP motor) these wrinkles affect the signal propagating to the detectors, limiting our ability to determine the polarization angles. Efforts to improve the uniformity of the grid in fabrication and mounting are ongoing.

5. COMPARISON TO EB NULLING

The polarization angle calibration presented in Section 3 is the approach used in Naess et al. 2014 and for all ACTPol results thus far.¹⁵ After implementing this calibration approach, Naess et al. 2014 tested the

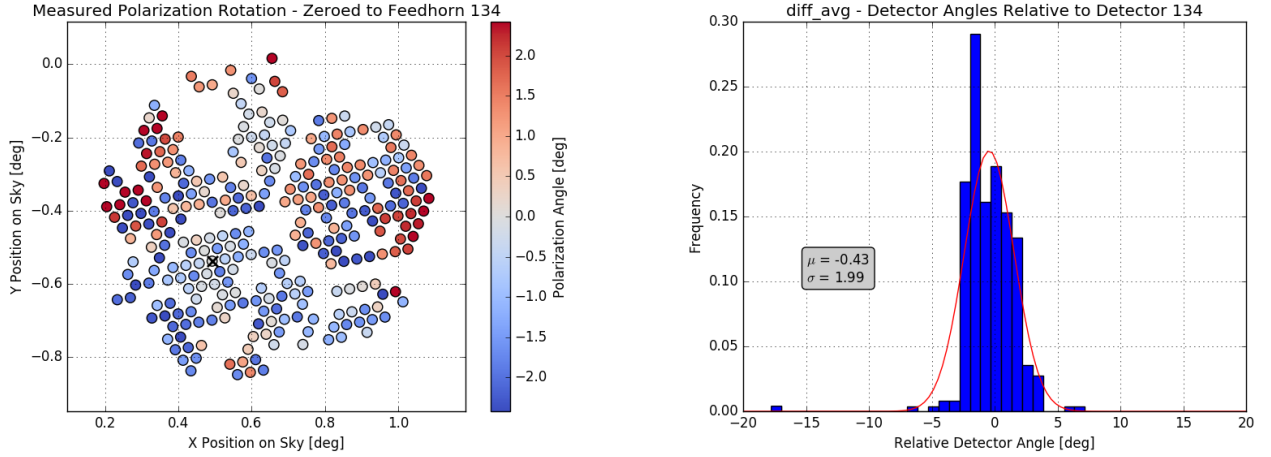


Figure 8. (Left): Measured polarization rotations relative to detector 134, marked with an 'X' on this plot. (Right): Histogram of average detector angles relative to detector 134 and its colocated partner, which are used as a reference.

polarization angle calibration by checking the EB nulling angle and found it to be $\delta\gamma_p = -0.2^\circ \pm 0.5^\circ$.¹⁵ Without the polarization angle calibration corrections presented in Section 3, degree scale corrections would have been required to null EB in Naess et al. 2014. This suggests that the optical modeling correctly captures the largest scale polarization angle corrections with a measurement uncertainty of $\pm 0.5^\circ$. Our best polarization grid measurements thus far have achieved a scatter of $\pm 2^\circ$. We plan to pursue better astrophysical measurements and polarization grid measurements to understand the calibration and test the modeling more precisely.

6. SUMMARY

We have outlined the steps taken to calibrate the ACTPol detector polarization angles. Working from the fabricated design angles we use planet observations to determine the installation angle and match these to our model for the optical distortions. Finally, we add the additional polarization rotation determined from optical modeling. This calibration technique has produced detector angles consistent with a global offset angle from zero when compared to the EB-nulling offset angle and is currently used to calibrate the ACTPol detectors.

A technique for measuring the polarization rotation due to the reimaging optics is also described. We observe a rotating polarization grid, fit the detector time streams to determine the detector angles and take the difference of this measured angle with the expected detector angle. The measured angles demonstrate the potential for this technique to constrain polarization rotation present in the reimaging optics; however, improvements need to be made with respect to the uniformity of the polarization grid to achieve sub-degree measurements of individual detector angles.

ACKNOWLEDGMENTS

The work of BJK, KPC, KTC, EG, CM, BLS, JTW, and SMS was supported by NASA Space Technology Research Fellowship awards. This work was supported by the U.S. National Science Foundation through award 1440226. The development of multichroic detectors and lenses was supported by NASA grants NNX13AE56G and NNX14AB58G. MDN acknowledges support from NSF award AST-1454881.

REFERENCES

- [1] Fowler, J. W., Niemack, M. D., Dicker, S. R., Aboobaker, A. M., Ade, P. A. R., Battistelli, E. S., Devlin, M. J., Fisher, R. P., Halpern, M., Hargrave, P. C., Hincks, A. D., Kaul, M., Klein, J., Lau, J. M., Limon, M., Marriage, T. A., Mauskopf, P. D., Page, L., Staggs, S. T., Swetz, D. S., Switzer, E. R., Thornton, R. J., and Tucker, C. E., “Optical design of the Atacama Cosmology Telescope and the Millimeter Bolometric Array Camera,” *Appl. Opt.* **46**, 3444–3454 (June 2007).

- [2] Thornton, R. J., Ade, P. A. R., Aiola, S., Angile, F. E., Amiri, M., Beall, J. A., Becker, D. T., Cho, H., Choi, S. K., Corlies, P., Coughlin, K. P., Datta, R., Devlin, M. J., Dicker, S. R., Dunner, R., Fowler, J. W., Fox, A. E., Gallardo, P. A., Gao, J., Grace, E., Halpern, M., Hasselfield, M., Henderson, S. W., Hilton, G. C., Hincks, A. D., Ho, S. P., Hubmayr, J., Irwin, K. D., Klein, J., Koopman, B., Li, D., Louis, T., Lungu, M., Maurin, L., McMahon, J., Munson, C. D., Naess, S., Nati, F., Newburgh, L., Nibarger, J., Niemack, M. D., Niraula, P., Nolte, M. R., Page, L. A., Pappas, C. G., Schillaci, A., Schmitt, B. L., Sehgal, N., Sievers, J. L., Simon, S. M., Staggs, S. T., Tucker, C., Uehara, M., van Lanen, J., Ward, J. T., and Wollack, E. J., “The Atacama Cosmology Telescope: The polarization-sensitive ACTPol instrument,” *ArXiv e-prints* (May 2016).
- [3] Lue, A., Wang, L., and Kamionkowski, M., “Cosmological signature of new parity-violating interactions,” *Phys. Rev. Lett.* **83**, 1506–1509 (Aug 1999).
- [4] Carroll, S. M., “Quintessence and the Rest of the World: Suppressing Long-Range Interactions,” *Physical Review Letters* **81**, 3067–3070 (Oct. 1998).
- [5] Leahy, J. P., “Comment on the Measurement of Cosmological Birefringence,” *ArXiv Astrophysics e-prints* (Apr. 1997).
- [6] Wardle, J. F. C., Perley, R. A., and Cohen, M. H., “Observational evidence against birefringence over cosmological distances,” *Phys. Rev. Lett.* **79**, 1801–1804 (Sep 1997).
- [7] Götz, D., Laurent, P., Antier, S., Covino, S., D’Avanzo, P., D’Elia, V., and Melandri, A., “GRB 140206A: the most distant polarized gamma-ray burst,” *MNRAS* **444**, 2776–2782 (Nov. 2014).
- [8] Komatsu, E., Smith, K. M., Dunkley, J., Bennett, C. L., Gold, B., Hinshaw, G., Jarosik, N., Larson, D., Nolte, M. R., Page, L., Spergel, D. N., Halpern, M., Hill, R. S., Kogut, A., Limon, M., Meyer, S. S., Odegard, N., Tucker, G. S., Weiland, J. L., Wollack, E., and Wright, E. L., “Seven-year Wilkinson Microwave Anisotropy Probe (WMAP) Observations: Cosmological Interpretation,” *ApJS* **192**, 18 (Feb. 2011).
- [9] Kaufman, J. P., Keating, B. G., and Johnson, B. R., “Precision tests of parity violation over cosmological distances,” *MNRAS* **455**, 1981–1988 (Jan. 2016).
- [10] Kamionkowski, M., Kosowsky, A., and Stebbins, A., “A probe of primordial gravity waves and vorticity,” *Phys. Rev. Lett.* **78**, 2058–2061 (Mar 1997).
- [11] Zaldarriaga, M. and Seljak, U., “All-sky analysis of polarization in the microwave background,” *Phys. Rev. D* **55**, 1830–1840 (Feb. 1997).
- [12] Hinshaw, G., Larson, D., Komatsu, E., Spergel, D. N., Bennett, C. L., Dunkley, J., Nolte, M. R., Halpern, M., Hill, R. S., Odegard, N., Page, L., Smith, K. M., Weiland, J. L., Gold, B., Jarosik, N., Kogut, A., Limon, M., Meyer, S. S., Tucker, G. S., Wollack, E., and Wright, E. L., “Nine-year Wilkinson Microwave Anisotropy Probe (WMAP) Observations: Cosmological Parameter Results,” *ApJS* **208**, 19 (Oct. 2013).
- [13] Keating, B. G., Shimon, M., and Yadav, A. P. S., “Self-calibration of Cosmic Microwave Background Polarization Experiments,” *ApJ* **762**, L23 (Jan. 2013).
- [14] Datta, R., Munson, C. D., Niemack, M. D., McMahon, J. J., Britton, J., Wollack, E. J., Beall, J., Devlin, M. J., Fowler, J., Gallardo, P., Hubmayr, J., Irwin, K., Newburgh, L., Nibarger, J. P., Page, L., Quijada, M. A., Schmitt, B. L., Staggs, S. T., Thornton, R., and Zhang, L., “Large-aperture wide-bandwidth antireflection-coated silicon lenses for millimeter wavelengths,” *Appl. Opt.* **52**, 8747 (Dec. 2013).
- [15] Naess, S., Hasselfield, M., McMahon, J., Niemack, M. D., Addison, G. E., Ade, P. A. R., Allison, R., Amiri, M., Battaglia, N., Beall, J. A., de Bernardis, F., Bond, J. R., Britton, J., Calabrese, E., Cho, H.-m., Coughlin, K., Crichton, D., Das, S., Datta, R., Devlin, M. J., Dicker, S. R., Dunkley, J., Dunner, R., Fowler, J. W., Fox, A. E., Gallardo, P., Grace, E., Gralla, M., Hajian, A., Halpern, M., Henderson, S., Hill, J. C., Hilton, G. C., Hilton, M., Hincks, A. D., Hlozek, R., Ho, P., Hubmayr, J., Hufenberger, K. M., Hughes, J. P., Infante, L., Irwin, K., Jackson, R., Muya Kasanda, S., Klein, J., Koopman, B., Kosowsky, A., Li, D., Louis, T., Lungu, M., Madhavacheril, M., Marriage, T. A., Maurin, L., Menanteau, F., Moodley, K., Munson, C., Newburgh, L., Nibarger, J., Nolte, M. R., Page, L. A., Pappas, C., Partridge, B., Rojas, F., Schmitt, B. L., Sehgal, N., Sherwin, B. D., Sievers, J., Simon, S., Spergel, D. N., Staggs, S. T., Switzer, E. R., Thornton, R., Trac, H., Tucker, C., Uehara, M., Van Engelen, A., Ward, J. T., and Wollack, E. J., “The Atacama Cosmology Telescope: CMB polarization at $200 < l < 9000$,” *J. Cosmology Astropart. Phys.* **10**, 7 (Oct. 2014).